Band Power Spectra in the *COBE*[1] DMR 4-Year Anisotropy Maps

G. Hinshaw[2,3], A.J. Banday[2,4], C.L. Bennett[5], K.M. Górski[2,6], A. Kogut[2],
G.F. Smoot[7,8] & E.L. Wright[9]

ABSTRACT

We employ a pixel-based likelihood technique to estimate the angular power spectrum of the *COBE* Differential Microwave Radiometer (DMR) 4-year sky maps. The spectrum is consistent with a scale-invariant power-law form with a normalization, expressed in terms of the expected quadrupole anisotropy, of $Q_{rms-PS|n=1} = 18 \pm 1.4$ μK, and a best-fit spectral index of 1.2 ± 0.3. The normalization is somewhat smaller than we concluded from the 2-year data, mainly due to additional Galactic modeling. We extend the analysis to investigate the extent to which the "small" quadrupole observed in our sky is statistically consistent with a power-law spectrum. The most likely quadrupole amplitude is somewhat dependent on the details of Galactic foreground subtraction and data selection, ranging between 7 and 10 μK, but in no case is there compelling evidence that the quadrupole is too small to be consistent with a power-law spectrum. We conclude with a likelihood analysis of the band power amplitude in each of four spectral bands between $\ell = 2$ and 40, and find no evidence for deviations from a simple power-law spectrum.

Subject headings: cosmic microwave background — cosmology: observations

---

[1]The National Aeronautics and Space Administration/Goddard Space Flight Center (NASA/GSFC) is responsible for the design, development, and operation of the Cosmic Background Explorer (*COBE*). Scientific guidance is provided by the *COBE* Science Working Group. GSFC is also responsible for the development of the analysis software and for the production of the mission data sets.

[2]Hughes STX Corporation, Laboratory for Astronomy and Solar Physics, Code 685, NASA/GSFC, Greenbelt MD 20771.

[3]e-mail: hinshaw@stars.gsfc.nasa.gov

[4]Current address: Max Planck Institut fur Astrophysik, 85740 Garching Bei Munchen Germany.

[5]Laboratory for Astronomy and Solar Physics, Code 685, NASA/GSFC, Greenbelt MD 20771.

[6]On leave from Warsaw University Observatory, Aleje Ujazdowskie 4, 00-478 Warszawa, Poland.

[7]Department of Physics, U.C. Berkeley, Berkeley, CA 94720.

[8]Lawrence Berkeley Laboratory, Bldg 50-351, University of California, Berkeley CA 94720.

[9]UCLA Astronomy, P.O. Box 951562, Los Angeles CA 90095-1562.

1. Introduction

The detection of large angular scale anisotropies in the Cosmic Microwave Background (CMB) radiation was first reported by the *COBE*-DMR experiment in 1992 (Smoot et al. 1992; Bennett et al. 1992; Wright et al. 1992; Kogut et al. 1992). The initial detection was based only on the first year of flight data. Since that time the DMR Team processed and analyzed the first two years of data and found results to be consistent with the first year results (Bennett et al. 1994, Górski et al. 1994, Wright et al. 1994a). We have now processed and analyzed the full 4-years of DMR observations: this paper is one of a series describing the results of our analysis. The maps and an overview of the scientific results are given in Bennett et al. (1996).

In this paper we analyze the angular power spectrum of the 4-year DMR maps using a pixel based likelihood technique which was first applied to the 2-year data by Tegmark & Bunn (1995). We extend previous work by considering several parameterization of the angular power spectrum. The simplest model for large angular scale anisotropy is the power-law model parameterized by a normalization, Q_{rms-PS}, and spectral index, n. It is of interest to separate the quadrupole anisotropy from the rest of the power spectrum since it is most plausibly contaminated by Galactic emission, and, in some models, is predicted to deviate from the simple power-law form. We extend our likelihood analysis to a three parameter model in which the quadrupole is fit independent of the higher-order power (which is assumed to follow a power-law, see §4 for details). Lastly we consider band power estimates in which the anisotropy is assumed to be scale-invariant in each of four modestly narrow ℓ bands, chosen to have roughly comparable sensitivity. The results are compared to the power-law fits and indicate that the anisotropy has no significant deviation from a power-law form.

2. Data Selection

The DMR experiment has produced two independent microwave maps (A and B) at each of 3 frequencies (31.5, 53 and 90 GHz). The results presented here are based on linear combinations of all 6 channel maps. The combination coefficients are dictated by the sensitivities of the individual channels and on considerations of Galactic foreground removal. Kogut et al. (1996a,1996b) have revisited the question of Galactic emission in the 2- and 4-year DMR data at high latitudes, and conclude that there is statistically significant evidence for a weak Galactic signal at all three frequencies, even at latitudes $|b| \geq 20°$. Thus, for the 4-year analysis, we take a more aggressive approach to Galactic foreground removal than we have previously: first, we extend the Galactic plane cut of 20° with additional cuts, guided by the *COBE*-DIRBE 140 μm map (Bennett et al. 1996). The number of pixels surviving the cut is 3881 in Galactic coordinates. Second, we model and remove residual high-latitude Galactic emission in two complementary ways, described

below. In all, we analyze three separate maps in this paper: the first map is a weighted average of all six DMR channel maps with no residual Galaxy emission subtracted. We denote this map "31+53+90". The second is the same weighted average map as the first with best-fit Galaxy template maps subtracted from each channel prior to averaging (Kogut et al. 1996b). We denote this the "Correlation" model map. The third is a linear combination of all six channels with coefficients designed to maximize sensitivity subject to the constraint that any signal with a free-free frequency spectrum ($\beta_{ff} = -2.15$) cancels. This map also has best-fit synchrotron and dust emission templates subtracted prior to averaging (Kogut et al. 1996b). We denote this the "Combination" model map. The specific coefficients used to construct these maps are given in Table 1 of Hinshaw et al. (1996). In all the analyses below we use the maps pixelized in Galactic coordinates. Górski et al. (1996) and Banday et al. (1996) have analyzed both the Galactic and ecliptic maps in detail. Since our results for the Galactic maps are in agreement with theirs, where comparable, we defer to those papers for a comparison of the Galactic and ecliptic maps.

3. Method

Most cosmological models make predictions for the mean angular power spectrum of CMB anisotropies, the coefficients, C_ℓ. For a rotationally invariant theory, the C_ℓ specify the expected variance in each spherical harmonic mode in a Fourier expansion of the sky temperature $T(\theta, \phi) = \sum_{\ell,m} a_{\ell m} Y_{\ell m}(\theta, \phi)$ with $\langle a_{\ell m} a_{\ell' m'}^* \rangle = C_\ell \, \delta_{\ell\ell'} \, \delta_{mm'}$. For a given power spectrum, C_ℓ, the implied covariance between map pixels i and j is given by

$$M_{ij} = \langle T_i T_j \rangle = \frac{1}{4\pi} \sum_\ell (2\ell + 1) \, W_\ell^2 \, C_\ell \, P_l(\hat{n}_i \cdot \hat{n}_j) \tag{1}$$

where T_i is the temperature in pixel i of a map, the angled brackets denote a universal ensemble average, W_ℓ^2 is the experimental window function that includes the effects of beam smoothing and finite pixel size, C_ℓ is the power spectrum, $P_l(\hat{n}_i \cdot \hat{n}_j)$ is the Legendre polynomial of order ℓ, and $\hat{n}_i$ is the unit vector towards the center of pixel i. For Gaussian fluctuations, the covariance matrix fully specifies the statistics of the temperature fluctuations. The probability of observing a map with pixel temperatures $\vec{T}$, given a power spectrum C_ℓ, is

$$P(\vec{T}|C_\ell) \, d\vec{T} = \frac{d\vec{T}}{(2\pi)^{N/2}} \, \frac{e^{-\frac{1}{2}\vec{T}^T \cdot M(C_\ell)^{-1} \cdot \vec{T}}}{\sqrt{\det M(C_\ell)}} \tag{2}$$

where N is the number of pixels in the map. Assuming a uniform prior distribution of cosmological model parameters, the probability of a power spectrum C_ℓ, given a map $\vec{T}$, is then

$$\mathcal{L}(C_\ell|\vec{T}) \propto \frac{e^{-\frac{1}{2}\vec{T}^T \cdot M^{-1}(C_\ell) \cdot \vec{T}}}{\sqrt{\det M(C_\ell)}}. \tag{3}$$

In the following section, we evaluate the above likelihood function using three different parameterizations of the power spectrum, C_ℓ. To test the effects of data selection and Galaxy modeling, we analyze three separate DMR maps, as specified in §2. To make the analysis computationally efficient, we have degraded the maps by one step in pixel resolution (to index level 5) for which there are 1536 pixels in the full sky, and 954 pixels surviving the extended Galaxy cut. We account for the effects of smoothing due to pixelization by including a term in the window function: $W_\ell = G_\ell F_\ell$. The G_ℓ are the Legendre coefficients of the DMR beam pattern, tabulated by Wright et al. (1994b). The F_ℓ are the Legendre coefficients for a circular top-hat function with area equal to the pixel area. The coefficients for index level 5 pixels are available on request.

We ignore the contribution of the monopole and dipole moments in the maps since these modes are either unconstrained by the data (the monopole), or are dominated by local effects (the dipole). In principle, this is achieved by integrating the likelihood over the modes C_0 and C_1; in practice, we set these terms to large positive constants when evaluating the covariance matrix. We have found that setting $C_0 = C_1 = 10^8$ μK^2 renders the likelihood insensitive to monopole and dipole moments of several hundred μK, without compromising the inversion of the covariance matrices. (Note that the analyzed maps have approximately zero mean, by construction, and approximately zero dipole since an estimate of the CMB dipole is removed during the raw data processing.) We assume the noise in the sky maps is uncorrelated from pixel to pixel (Lineweaver et al. 1994), which adds a diagonal contribution to the pixel covariance matrix in Equation 1. Tegmark & Bunn (1995) have shown the assumption of uncorrelated noise to be an excellent approximation for this application. The noise per pixel is derived from the noise per observation, given in Table 1 of Bennett et al. (1996), and the number of observations per pixel.

4. Results

We consider three parameterizations of the angular power spectrum. First, we adopt the power-law model, parameterized by the amplitude of the mean quadrupole anisotropy, Q_{rms-PS}, and the power-law spectral index n. Specifically (Bond & Efstathiou, 1987)

$$C_\ell = C_\ell(Q_{rms-PS}, n) \equiv (4\pi/5)Q_{rms-PS}^2 \frac{\Gamma(\ell + (n-1)/2)\Gamma((9-n)/2)}{\Gamma(\ell + (5-n)/2)\Gamma((3+n)/2)} \tag{4}$$

This model is extended to study the quadrupole anisotropy by parameterizing the power at $\ell = 2$ separately

$$C_\ell = \begin{cases} C_2 & \ell = 2 \\ C_\ell(Q_{rms-PS}, n) & \ell \geq 3 \end{cases} \tag{5}$$

The most-likely value of C_2 that results from this model is closely related to the quadrupole anisotropy observed in our sky, which we denote Q_{rms}; the precise connection is discussed below. Note also that the power-law parameters, Q_{rms-PS} and n, inferred from this model are essentially

the same as those derived from marginalizing over C_2 since they are only weakly coupled to C_2. Lastly, we study a model in which the spectrum is taken to be scale-invariant in each of four relatively narrow ℓ bands, and let the amplitude in each be a free parameter

$$
\ell(\ell+1)\,C_\ell = \left\{
\begin{array}{ll}
(24\pi/5)\,Q_\alpha^2 & 2 \leq \ell \leq 5 \\
(24\pi/5)\,Q_\beta^2 & 6 \leq \ell \leq 10 \\
(24\pi/5)\,Q_\gamma^2 & 11 \leq \ell \leq 20 \\
(24\pi/5)\,Q_\delta^2 & 21 \leq \ell \leq 40
\end{array}
\right.
\tag{6}
$$

Note that within each band, the amplitude parameters $Q_{\alpha\cdots\delta}$ correspond to Q_{flat} as defined by Scott, Silk & White (1995). The spectral band widths were chosen to give roughly equal sensitivity in each band except the highest which suffers loss of signal due to the $7°$ beam width. The model is designed to probe for deviations from a power-law while maintaining computational feasibility.

The fits to power-law spectra, including the quadrupole in the analysis, are summarized in Table 1. The results are generally consistent with the 2-year data. The overall normalization is slightly smaller due to the additional Galactic cutting and modeling. The most-likely spectral index is slightly greater than unity, while the quadrupole normalization for a scale-invariant spectrum ranges from 17.2 to 18.4 μK, depending on Galactic model. For comparison, the scale-invariant normalization derived from the weighted average map using a straight $20°$ cut with no additional Galactic modeling is 20.1 μK, 1.6 μK higher than we obtain with the extended cut, and comparable to the normalization quoted by Górski et al. (1994) for the 2-year data (using a straight cut). In assessing the results obtained from the three maps, we note that the DIRBE 140 μm map appears to trace the bulk of the free-free emission seen by DMR (Kogut et al. 1996b), and since the Correlation map is more sensitive than the Combination map, we give it more weight in our conclusions. Taken together, the results in Table 1 are consistent with a spectral index of 1.2 ± 0.3 and a scale-invariant quadrupole normalization of 18 ± 1.4 μK.

The fits to power-law spectra with the quadrupole parameterized independently are summarized in Table 2. The first three columns summarize the power-law portion of the spectrum in the same format as Table 1. These results are based on slicing the 3-dimensional likelihood at the maximum likelihood value for C_2, but the results are only weakly dependent on C_2 and thus are effectively equivalent to standard power-law fits that ignore the quadrupole. The last column of Table 2 gives the 68% confidence interval for C_2 expressed in terms of $Q_{rms} \equiv \sqrt{(5/4\pi)C_2}$. The mode gives a self-consistent estimate of the quadrupole moment observed in our sky, while the confidence range accounts for both instrument noise *and* cosmic variance. A complimentary approach to analyzing the quadrupole, based on fitting and squaring a_{2m} coefficients (Kogut et al. 1996b) gives consistent results, after accounting for the bias introduced by uncertainties in the a_{2m}. This approach demonstrates the importance of modeling the residual galactic foreground emission since it contributes significantly to the quadrupole emission. As with previous analyses, the observed quadrupole is smaller than that expected from the power-law fits: the most-likely amplitude ranges from 6.9 to 10.0 μK depending on Galaxy model. Figure 1 shows the full likelihood for Q_{rms} for each map analyzed. It is important to stress that while the quadrupole in

our sky is most likely $\sim$10 μK, the cosmic variance combined with experimental uncertainties are so large that its value is easily consistent with a power-law model of anisotropy. For example, the likelihood for Q_{rms} derived from the Correlation map implies there is a 22% chance that Q_{rms} exceeds 18 μK, the value favored in a scale-invariant power-law model.

The band power fits are summarized in Table 3, and are plotted in Figure 2. The vertical uncertainties in the figure indicate the extent of the 68% confidence interval in each band power parameter when the other 3 are fixed at their maximum likelihood value. These uncertainties include both instrument noise and cosmic variance. The horizontal errors bars represent the extent of each band, as defined in Equation 6. The covariance between bands, which arises from the Galaxy cut and from non-uniform sky coverage, is quite small: roughly 10% of the parameter variance for neighboring bands, and less for non-neighboring bands. Note that each of the three lowest bands have consistently significant detections of power, while, in all cases, the highest band, from 21 to 40, does not. Thus, we only plot 95% confidence upper limits for this band. To compare the band power fits to the power-law fits we have also plotted the 68% confidence locus of acceptable power-law models in Figure 2. More precisely, the dashed white line in the figure is the mean power spectrum for the most-likely power-law model, while the grey band represents the locus of mean power spectra within the 68% confidence region in the (Q_{rms-PS}, n) plane. The general agreement between the power-law model and the band power model is an indication that there are no significant wide band deviations (with $\Delta\ell \sim$ a few) from a simple power-law in the low-ℓ anisotropy spectrum. The band power amplitude in the highest ℓ band we probe is consistently low, but this estimate is rather sensitive to the details of the beam and pixelization filters, and to the level of noise in the maps, so the uncertainty attached to this estimate is quite large. To date, two other experiments have measured anisotropy on angular scales probed by the DMR: FIRS (Ganga et al. 1994) and Tenerife (Hancock et al. 1994). Both experiments report significant detections of anisotropy: the FIRS team quotes $Q_{flat} = 19 \pm 5$ μK for $\ell \lesssim 30$, while the Tenerife team quotes $Q_{flat} = 26 \pm 6$ μK for $13 \lesssim \ell \lesssim 30$, both of which are consistent with DMR.

5. Conclusions

We have estimated various parameterizations of the angular power spectrum in the *COBE*-DMR 4-year sky maps. We find the results to be generally consistent with the first and second year results. The data are consistent with a scale-invariant spectrum with a quadrupole normalization of 18 ± 1.4 μK, and a best-fit spectral index of 1.2 ± 0.3. The quadrupole anisotropy is somewhat smaller than the best-fit power-law spectrum would prefer, but the discrepancy is not statistically significant when we take account of Galactic modeling uncertainties, instrument noise, and cosmic variance. We have further analyzed the spectrum in each of four ℓ bands and find no evidence for significant, wide-band deviations from a simple power-law form.

Table 1.   Power-law Spectral Parameters

Map	n[a]	Q_{rms-PS}[b] (μK)	$Q_{rms-PS\|n=1}$[c] (μK)
31+53+90[d]	$1.25^{+0.26}_{-0.29}$	$15.4^{+3.9}_{-2.9}$	$18.4^{+1.4}_{-1.3}$
Correlation[d]	$1.23^{+0.26}_{-0.27}$	$15.2^{+3.6}_{-2.8}$	$17.8^{+1.3}_{-1.3}$
Combination[d]	$1.00^{+0.40}_{-0.43}$	$17.2^{+5.6}_{-4.0}$	$17.2^{+1.9}_{-1.7}$

[a]Mode and $\pm 68\%$ confidence interval for the projection of the 2-dimensional likelihood $\mathcal{L}(Q_{rms-PS}, n)$ on to n.

[b]Mode and $\pm 68\%$ confidence interval for the projection of the 2-dimensional likelihood $\mathcal{L}(Q_{rms-PS}, n)$ on to Q_{rms-PS}.

[c]Mode and $\pm 68\%$ confidence interval for the slice of the 2-dimensional likelihood $\mathcal{L}(Q_{rms-PS}, n)$ at $n = 1$.

[d]Linear combination coefficients for the maps analyzed here are given in Table 1 of Hinshaw et al. (1996).

Table 2. Quadrupole + Power-law Spectral Parameters

Map	n[a]	Q_{rms-PS}[b] (μK)	$Q_{rms-PS\|n=1}$[c] (μK)	Q_{rms}[d] (μK)
31+53+90[e]	$1.09^{+0.29}_{-0.30}$	$17.5^{+4.7}_{-3.6}$	$18.7^{+1.4}_{-1.3}$	$6.9^{+5.4}_{-2.7}$
Correlation[e]	$1.09^{+0.29}_{-0.31}$	$17.0^{+4.7}_{-3.6}$	$18.1^{+1.4}_{-1.3}$	$10.0^{+6.5}_{-4.4}$
Combination[e]	$0.57^{+0.44}_{-0.49}$	$23.0^{+8.4}_{-5.7}$	$17.9^{+1.9}_{-1.8}$	$7.6^{+6.2}_{-4.5}$

[a]Mode and $\pm68\%$ confidence interval for the projection of the 2-dimensional likelihood $\mathcal{L}(Q_{rms-PS}, n)$ on to n. $\mathcal{L}(Q_{rms-PS}, n)$ is the 3-dimensional likelihood $\mathcal{L}(Q_{rms}, Q_{rms-PS}, n)$ evaluated at the maximum likelihood value of Q_{rms}.

[b]Mode and $\pm68\%$ confidence interval for the projection of the 2-dimensional likelihood $\mathcal{L}(Q_{rms-PS}, n)$ on to Q_{rms-PS}.

[c]Mode and $\pm68\%$ confidence interval for the slice of the 2-dimensional likelihood $\mathcal{L}(Q_{rms-PS}, n)$ at $n = 1$.

[d]Mode and $\pm68\%$ confidence interval for the slice of the 3-dimensional likelihood $\mathcal{L}(Q_{rms}, Q_{rms-PS}, n)$ at the maximum likelihood values of Q_{rms-PS} and n. Similar results are obtained by marginalizing over Q_{rms-PS} and n.

[e]Linear combination coefficients for the maps analyzed here are given in Table 1 of Hinshaw et al. (1996).

Table 3.   Band Power Spectral Parameters[a]

| Map | —Band— | | | |
	$2 \leq \ell \leq 5$	$6 \leq \ell \leq 10$	$11 \leq \ell \leq 20$	$21 \leq \ell \leq 40$
31+53+90[b]	$18.6^{+4.5}_{-3.4}$	$16.7^{+2.4}_{-2.0}$	$20.3^{+2.2}_{-2.1}$	$1.0^{+13.2}_{-1.0}$
Correlation[b]	$18.0^{+3.6}_{-2.6}$	$15.9^{+2.3}_{-1.8}$	$19.9^{+2.2}_{-2.0}$	$0.8^{+12.6}_{-0.8}$
Combination[b]	$17.5^{+4.7}_{-3.7}$	$17.2^{+2.9}_{-2.5}$	$17.2^{+4.6}_{-4.7}$	$0.1^{+22.2}_{-0.1}$

[a]Mode and $\pm68\%$ confidence interval for the band power amplitudes, expressed in terms of Q_{flat}. Q_{flat} is the quadrupole normalization expected for a scale-invariant power-law spectrum within the specified range of ℓ. The units are μK.

[b]Linear combination coefficients for the maps analyzed here are given in Table 1 of Hinshaw et al. (1996).

REFERENCES

Banday, A.J., et al. 1996, ApJ, in preparation

Bennett, C.L., et al. 1992, ApJ, 396, L7

Bennett, C.L., et al. 1994, ApJ, 436, 423

Bennett, C.L., et al. 1996, ApJ, submitted

Bond, J.R. & Efstathiou, G. 1987, MNRAS, 226, 655

Ganga, K., Page, L., Cheng, E.S. & Meyer, S. 1994, ApJ, 432, L15

Górski, K.M., Hinshaw, G., Banday, A.J., Bennett, C.L., Wright, E.L., Kogut, A., Smoot, G.F. & Lubin, P. 1994, ApJ, 430, L89

Górski, K.M., Banday, A.J., Bennett, C.L., Hinshaw, G., Kogut, A., Smoot, G.F. & Wright, E.L. 1996, ApJ, submitted

Hancock, S., Davies, R.D., Lasenby, A.N., Gutierrez de la Cruz, C.M., Watson, R.A., Rebolo, R. & Beckman, J.E. 1994, Nature, 367, 333

Hinshaw, G., Banday, A.J., Bennett, C.L., Górski, K.M., Kogut, A. Lineweaver, C.H., Smoot, G.F. & Wright, E.L. 1996, ApJ, submitted

Kogut, A., et al. 1992, ApJ, 401, 1

Kogut, A., Banday, A.J., Bennett, C.L., Górski, K.M., Hinshaw, G. & Reach, W.T. 1996a, ApJ, 460, in press

Kogut, A., Hinshaw, G., Banday, A.J., Bennett, C.L., Górski, K.M., Smoot, G.F. & Wright, E.L. 1996b, ApJ, submitted

Lineweaver, C.H., et al. 1994, ApJ, 436, 452

Scott, D., Silk, J. & White, M. 1995, Science, 268, 829

Smoot, G.F., et al. 1992, ApJ, 396, L1

Tegmark, M. & Bunn, E.F. 1995, ApJ, 455, 1

Wright, E.L., et al. 1992, ApJ, 396, L13

Wright, E.L., Smoot, G.F., Bennett, C.L., & Lubin, P.M. 1994a, ApJ, 436, 443

Wright, E.L., Smoot, G.F., Kogut, A., Hinshaw, G., Tenorio, L., Lineweaver, C., Bennett, C.L., & Lubin, P.M. 1994b, ApJ, 420, 1
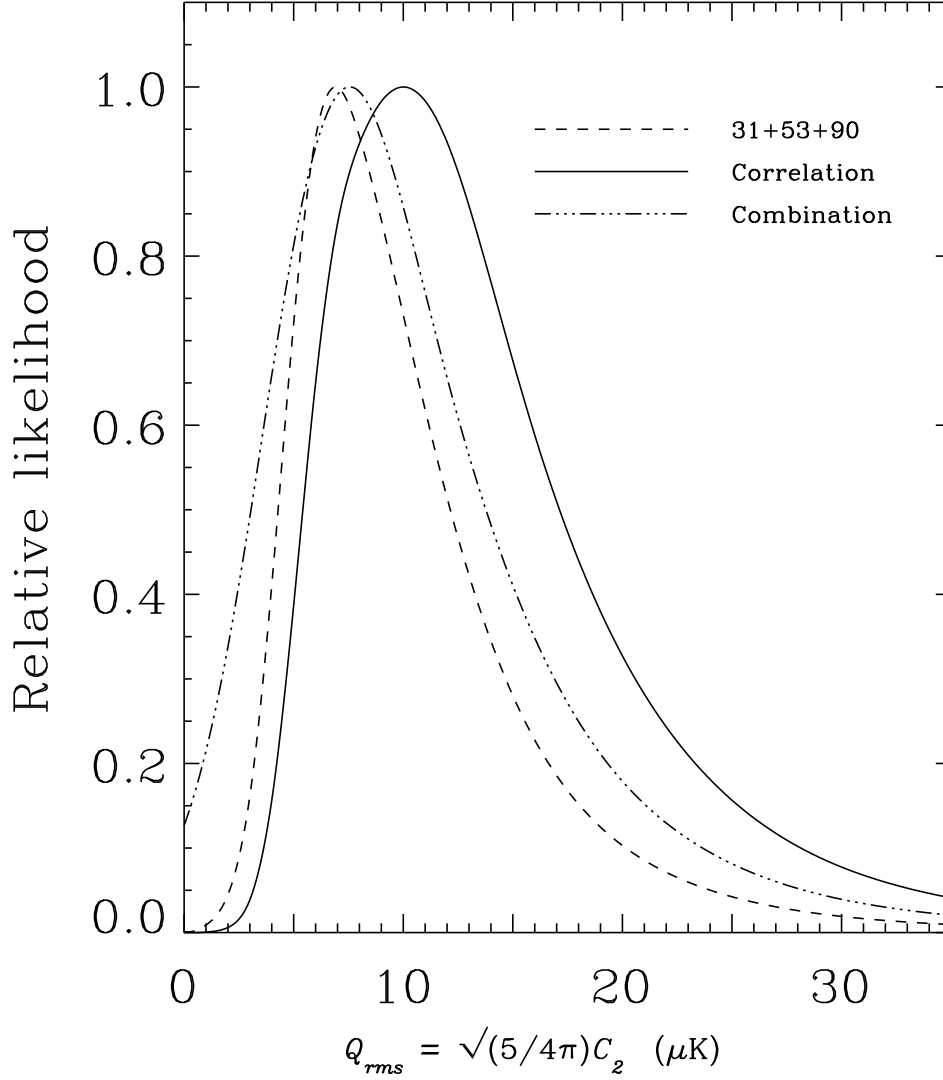
Fig. 1.— The likelihood function for the mean quadrupole moment observed in our sky for the three maps defined in §2. The curves include cosmic variance and instrument noise. In all cases the most likely quadrupole is smaller than that favored by the power-law fits to the full data, but the likelihoods are all sufficiently broad to encompass the case $Q_{rms} = Q_{rms-PS}$. The effect of Galactic modeling on Q_{rms} is relatively modest, but it does have a significant effect on the phase of the quadrupole, particularly the coefficient a_{20} (Kogut et al. 1996)
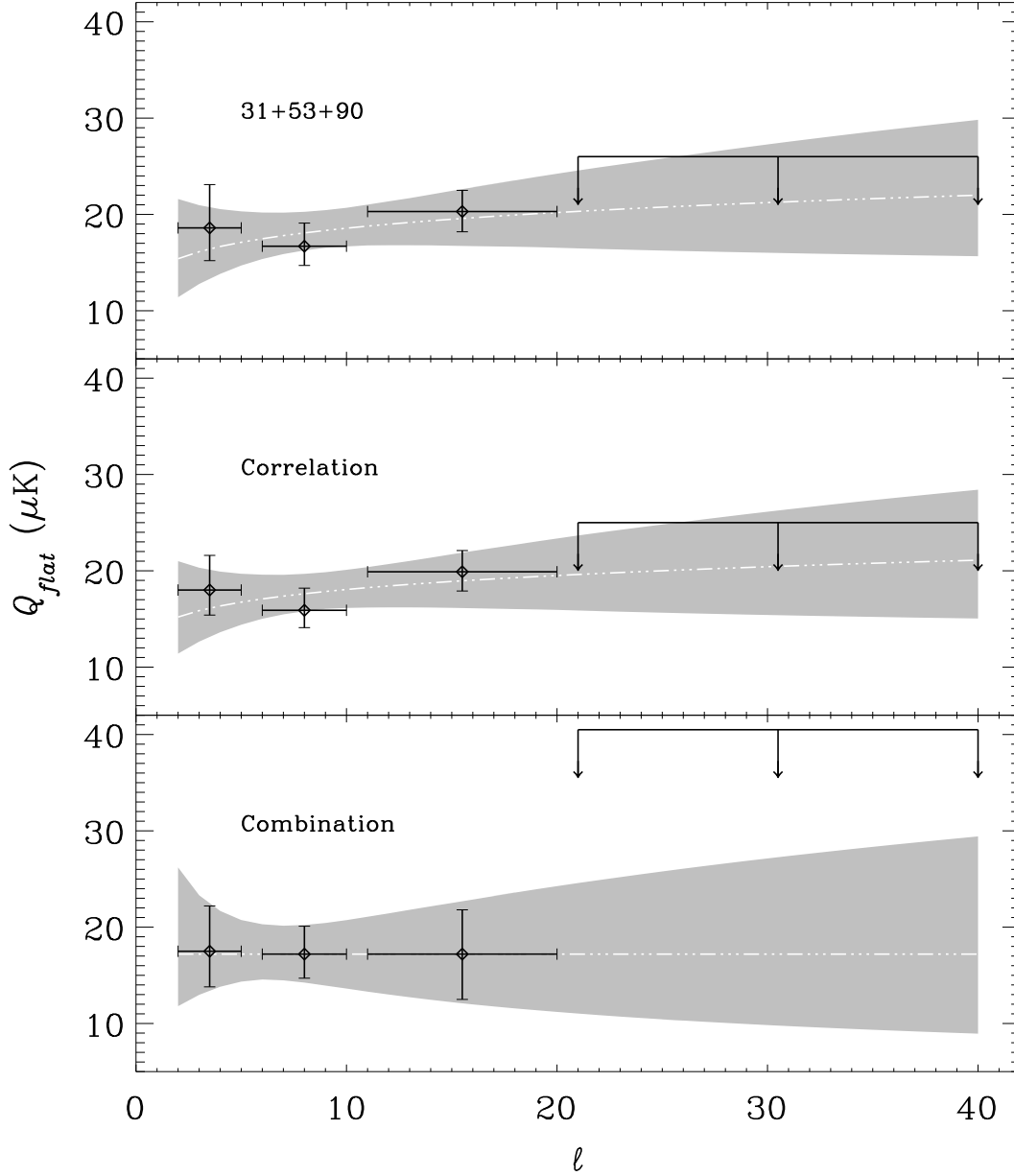
Fig. 2.— Power spectral estimates for three maps defined in §2. The points with error bars give the most likely band power amplitude within each ℓ band, as indicated by the horizontal error bars, under the assumption that the power spectrum is scale-invariant within each band. The fourth band, $21 \leq \ell \leq 40$, is plotted as a 95% CL upper limit, since there is no significant detection of power in this band. The vertical errors include both noise and cosmic variance. The shaded region indicates the locus of the mean of acceptable power-law models, i.e., those models within the 68% confidence region in the (Q_{rms-PS}, n) plane, as determined from the power-law fits to each map. The dashed white line within the shaded region gives the mean power spectrum for the most-likely